SPALLING AND MECHANICAL PROPERTIES OF HIGH STRENGTH CONCRETE AT HIGH TEMPERATURE

ECAILLAGE ET PROPRIETES MECANIQUES DES BETONS A HAUTES PERFORMANCES A TEMPERATURE ELEVEE

Long PHAN
National Institute of Standards and Technology, Gaithersburg, USA

ABSTRACT - Effects of elevated temperature exposure and various factors, including water-to-cementitious materials ratios (*w/cm*), curing conditions, heating rates, test methods, and polypropylene (PP) fibers, on (1) pore pressure buildup and potential for explosive spalling and on (2) degradation of mechanical properties in normal strength (NSC) and high-strength concrete (HSC) are presented. Degradations of mechanical properties were measured using 100 x 200 mm cylinders, heated to temperatures of up to 600 °C at 5 °C/min, and compared with results of other studies and existing codes. Pore pressures were measured using 100 x 200 x 200 mm blocks, heated to 600 °C at 5 °C/min and 25 °C/min. Experimental evidences of the complex, temperature-dependant moisture transport process which significantly influenced pore pressure and temperature developments are described.

RESUME – On présente dans cet article les effets de l'exposition à température élevée, et de différents paramètres parmi lesquels le rapport eau – liant, les conditions de cure, la vitesse de chauffe, la procédure expérimentale, et la teneur en fibres de polypropylène, sur 1° la montée en pression dans les pores constituant le potentiel vis-à-vis d'un écaillage explosif, et 2° sur la dégradation des propriétés mécaniques des bétons ordinaires et à haute résistance. La dégradation des propriétés mécaniques a été mesurée sur des cylindres 100 x 200 mm, chauffés à 5°C/mn jusqu'à des températures atteignant 600°C, et comparée aux résultats d'autres études et aux codes existants. La pression dans les pores a été mesurée dans des blocs 100 x 200 x 200 mm, chauffés jusqu'à 600 °C à raison de 5°C/mn ou 25°C/mn. On décrit les observations expérimentales liées au processus complexe du transport hydrique, dépendant de la température, qui a une influence sensible sur la pression dans les pores et l'histoire de température.

1. Introduction

It is now well known that short-term exposure to elevated temperature affects properties and behavior of HSC and NSC differently, and the differences are in two main areas: (1) strength loss in the intermediate temperature range (100 °C to 400 °C); and (2) occurrence of explosive spalling in HSC at similar range of temperatures. Both of these material behavioral differences have structural implications. First, the difference in relative strength loss between HSC and NSC at elevated temperature raise questions as to whether existing design rules prescribed in current codes for determining concrete strength at elevated temperatures, which were based primarily on tests of NSC, are applicable or safe for structures built with HSC. Second, the occurrence of explosive spalling at relatively low temperature, frequently observed for HSC, means HSC structural elements might sustain

loss of concrete cover protecting the steel reinforcements early in a fire, causing the steel reinforcements to be exposed directly to heating and leading to premature loss of overall structural capacity.

Explosive spalling, which refers to a sudden and violent breaking away of a surface layer concrete, has been observed in many laboratory tests of HSC specimens (Diederichs et al., 1995; Castillo and Durrani, 1990; Phan, 2005; Phan and Carino, 2003, 2002; Hertz, 1984; Kodur, 2003; Kalifa et al., 2000). This phenomenon has been generally attributed to the inability of HSC, due its low permeability, to successfully mitigate the buildup of internal pressure as free water residing in the concrete pores and chemically-bound water in the concrete matrix undergo transformation from liquid to a gaseous phase, expand in volume, and transport through the concrete with increasing concrete temperature.

Reports on factors affecting the degradation of HSC's mechanical properties and tendency for explosive spalling have been inconsistent (and sometimes contradictory), and a complete understanding of how these factors influence the behavior of HSC at elevated temperature has not had the benefit of quantifiable measurements. Given (1) the many benefits of HSC and its increased use in structural applications, and (2) the ongoing efforts to model the spalling behavior of HSC in fire, it is essential that behavior of HSC at elevated temperatures be understood to ensure that structural fire design involving HSC will be safe.

2. Experimental Program

The study includes two series of experiments. One measured concrete mechanical properties at elevated temperatures using 100 x 200 mm cylinders. The other measured the heat-induced internal pore pressures in concrete using 100 x 200 x 200 mm blocks.

In the mechanical property test series, the specimens were tested at steady-state temperature conditions using three test methods, namely *stressed*, *unstressed*, and *unstressed residual property* test methods. In the *stressed* and *unstressed* test methods, the specimens were subjected to simultaneous application of loading and heating and loaded to failure under uniaxial compression *at elevated temperatures*. In the *unstressed residual property* test method, the specimens were heated to target temperatures, allowed to cool to room temperature, and then loaded to failure *at room temperature*. In addition, *stressed* test specimens were restrained by a preload equal to 40 percent of their room-temperature compressive strength ($0.4f_{23oC}$) prior to and throughout the heating process (the *unstressed* and *unstressed residual property* test specimens were heated without preload).

In the pore pressure test series, the specimens were insulated on all sides, except the face, to simulate the one-dimensional heat flow condition that exists in a concrete wall exposed to fire, and were subjected only to heating without any mechanical loading.

2.1 Specimen Materials

The specimens of both test series were made using the same materials and mixture proportions (ASTM Type I Portland cement, 13 mm maximum size crushed limestone aggregate, natural sand with a fineness modulus of 2.85, silica fume (in the form of a slurry with a density of 1.42 g/cm^3 and a 54 % silica fume concentration), and high range water-reducing admixture). For the mechanical property test series, the specimens were made using four mixture proportions, designated mixtures I to IV (mixtures I to III are HSC,

mixture IV is NSC in Table 1). For the pore pressure test series, the specimens were made using two mixtures, I and IV (lowest and highest *w/cm* ratios). Some of the pore pressure specimens also contained commercially available monofilament PP fibers of two different lengths, 13 mm and 38 mm. The 13-mm long fiber has a diameter of 100 μm, and the 38-mm long fiber has a diameter of 300 μm. Both types of fibers have the same aspect ratio (125:1).

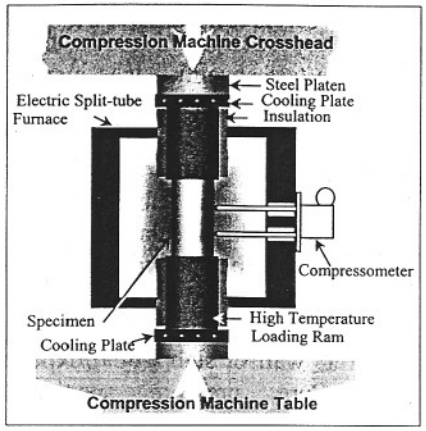

Figure 1- Mechanical property test setup

2.2 Instrumentation, Test Setup, and Heating Regimes

All specimens of the mechanical property test series were cured under water at room temperature until test time. Before testing, each specimen was instrumented with two type K thermocouples, one on the specimen's surface and one at the specimen's center. The thermocouples were used to determine whether the steady-state temperature condition has been achieved in the specimen (defined as the temperature condition where the difference between the temperatures on the specimen surface and center is within ± 5 °C). Fig. 1 shows the typical test setup for the mechanical property test series. The specimen was placed at the center of the electric split-tube furnace with openings at the top and bottom to allow the loading rams to transmit compressive load from the test machine. For the *unstressed residual property* tests, the cylinders were heated separately and allowed to cool down to room temperature before loading to failure (24 hours of natural cooling after heating).

Table 1. Mixture proportions and properties of concrete

		Mixture I (*w/cm*=0.22)	**Mixture II** (*w/cm*=0.33)	**Mixture III** (*w/cm*=0.33)	**Mixture IV** (*w/cm*=0.57)
Materials	Cement (kg/m^3)	596	596	662	376
	Water (kg/m^3)	133	199	194	213
	Coarse aggregate*(kg/m^3)	846	846	846	854
	Fine aggregate* (kg/m^3)	734	734	734	868
	Silica fume	66	66	0	0
	HRWRA** (mL/m^3)	400	354	154	0
Properties	***Fresh concrete***				
	Slump (mm)	240	230	35	76
	Air content (%)	3.2	2.8	2.0	2.5
	Hardened concrete				
	Initial moisture content (%)	5.0	6.1	6.3	7.3
	Compressive strength (MPa)				
	28-day	75.3	66.0	53.2	40.6
	400-day	98.2	81.2	72.3	46.9
	Dynamic Modulus (GPa)				
	400-day	47.2	43.7	44.1	36.7

* Saturated surface-dry condition **High-Range Water Reducing Admixture

Figure 2 shows the test setup for the pore pressure test series. Prior to heating, the pore pressure test specimen was insulated on all sides with an insulation blanket except on the heated face. The specimen was then placed at the center of a programmable electric furnace and subjected to heating by convection. The insulation promoted heat flow through the specimen, from the heated face to the insulated back face, similar to the one-directional heating condition that a concrete wall or slab would experience in a fire. Pore pressure specimens were instrumented with specialized pore pressure gages and also with type K thermocouples, which were co-located at points 25 mm, 50 mm, and 75 mm deep from the specimen's heated face. In addition, thermocouples were also placed on the front and back surfaces of the specimen. The pore pressure gages were made of a porous metal disc (1 mm thick with diameter of either 6 mm or 12 mm) crimped into a stainless steel cup of the same diameter. The stainless steel cup was welded to a stainless steel tube with an inner diameter of 1.6 mm. During concrete casting, the stainless steel cup (with the porous metal disc) was set at the desired depth in the concrete with the tube extending out of the backside of the specimen. The embedded stainless steel cup with porous metal disc allows the vapor pressure inside the concrete specimen to be transmitted through the porous metal disc and the tube. Before testing, the tube, which extends out of the specimen and the furnace, was connected to a miniature pressure transducer outside the furnace. The pressure transducers have a pressure range of 0 – 1000 psig and an uncertainty of ± 1%. The entire pore pressure assembly was filled by vacuum with high temperature silicone oil to facilitate the transfer of any vapor pressure developed inside the concrete to the miniature transducer.

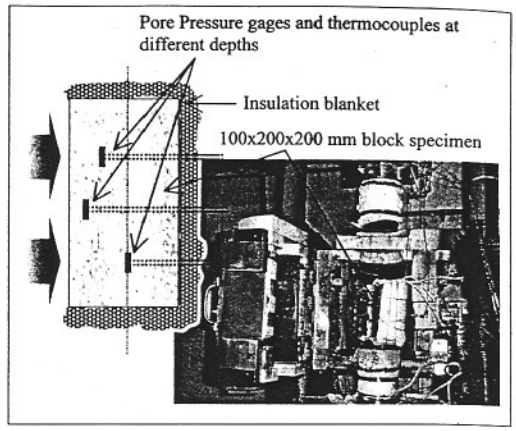

Figure 2- Pore pressure test setup

Two heating profiles - both impose a maximum furnace air temperature of 600 °C but at two different heating rates: 5 °C/min and 25 °C/min - were selected for the pore pressure test series. The test is terminated after explosive spalling occurs or after 5 hours of heating exposure, whichever occurs first.

2.3 Test Variables

The mechanical property test series was designed to study the effects of (1) test conditions (stressed, unstressed, and unstressed residual property tests); (2) *w/cm* ratios (0.22, 0.33, and 0.57); and (3) silica fume contents (0 % or 10 % cement replacement by mass) on mechanical properties of NSC and HSC at elevated temperature.

The pore pressure test series was designed to study the effects of (1) *w/cm* ratios; (2) dosages of PP fiber (0, 1.5 kg/m^3, and 3 kg/m^3); (3) PP fiber lengths (13 mm and 38 mm); (4) heating rates (5 °C/min and 25 °C/min); and (5) curing conditions (moist-cured by submergence and air-dried) on pore pressure buildup and potential for spalling of NSC and HSC. Table 2 shows the test matrix and key parameters of each of the pore pressure test specimen. Individual test specimens were named using the following convention:

Mixture # - Fiber Dosage - Fiber Length - Curing Condition - Heating Rate

(I or IV) (0, 1.5, or 3 kg/m^3) (13 or 38 mm) (Moist- or Air-cured) (5 or 25 °C/min)

Table 2 - Test matrix and specimen parameters for pore pressure test series

Test #	Specimen Name	Mixture (*w/cm*)	PP Fibers Dosage (kg/m^3)	PP Fibers Length (mm)	Curing Condition	Heating Rate (°C/min)
1	I-3-38-M-5	I (0.23)	3.0	38	Submerged	5
2	I-3-38-M-25					25
3	I-3-38-A-5				Air-dried	5
4	I-3-38-A-25					25
5	I-3-13-M-5			13	Submerged	5
6	I-3-13-M-25					25
7	I-3-13-A-25				Air-dried	25
8	I-1.5-38-M-5		1.5	38	Submerged	5
9	I-1.5-13-M-5			13		5
10	I-1.5-13-M-5 (*)					5
11	I-0-0-M-5		0	0	Submerged	5
12	I-0-0-M-5 (*)					5
13	I-0-0-M-25					25
14	I-0-0-A-5				Air-dried	5
15	I-0-0-A-25					25
16	IV-0-0-M-5	IV (0.57)	0	0	Submerged	5
17	IV-0-0-M-25					25
18	IV-0-0-A-5				Air-dried	5

(*) Duplicate specimens for repeatability

3. Test Results and Discussions

3.1 *Mechanical Property Test Series*

3.1.1 Strength-Temperature Relationships

The results of the mechanical property test series are shown as relative compressive strength ($f_{\theta\,c}/f_{23°C}$) versus temperature relationships in Figure 3. Also shown in these figures are results of other studies for comparison purposes. In these figures, the results of HSC are shown as solid lines, and the results of NSC are shown as dashed lines. The ranges of NIST test results are shaded for convenience.

Figure 3(a) shows the relative strength – temperature relationships for HSC and NSC under the stressed test method. The NIST test results showed that HSC sustained an average strength loss of slightly above 25 % at 100 °C. This is followed by a minor strength recovery when concrete reaches temperature between 100 °C and 450 °C (maximum strength recovery occurs at 300 °C). At temperature between 450 °C and 600 °C, the temperature rate of strength loss becomes more significant. Also, at temperature above 450 °C, all specimens of mixtures II and III failed due to explosive spalling (while being heated to 600 °C), resulting in unavailability of data for these two mixtures at above 450 °C. The NIST test results are consistent with results by Castillo and Durrani (1990) at up to 300 °C, and with results by Khoury and Algar (1999) at 100 °C. Results by Abrams (1971), however, indicated significantly different strength-temperature relationships for NSC. For

NSC with siliceous aggregate, test results by Abrams indicated that there was a slight strength gain at temperature up to 400 °C, and strength loss was not observed until concrete reaches temperature above 400 °C. For NSC with calcareous aggregate, no significant effect on strength due to temperature exposure was observed until 650 °C. Castillo and Durrani (1990) reported explosive spalling in about one third of the specimens being heated to 700 °C while Khoury and Algar (1999) did not mention explosive spalling. Further data may be found in Phan (2005, 2004) and Phan and Carino (2003, 2002).

Figure 3(b) shows the strength-temperature relationships for HSC and NSC under the unstressed test method. These relationships shown in the NIST's unstressed test data are similar in trend with those of the NIST's stressed test data, except that the strength losses in the unstressed tests are slightly larger at each target temperature. The NIST results also followed the general trend of unstressed HSC tests reported by Hammer (1995) and Diederichs et al. (1995), which constituted the majority of available unstressed test data for HSC. Almost all studies reported higher strength loss for HSC compared to NSC within the

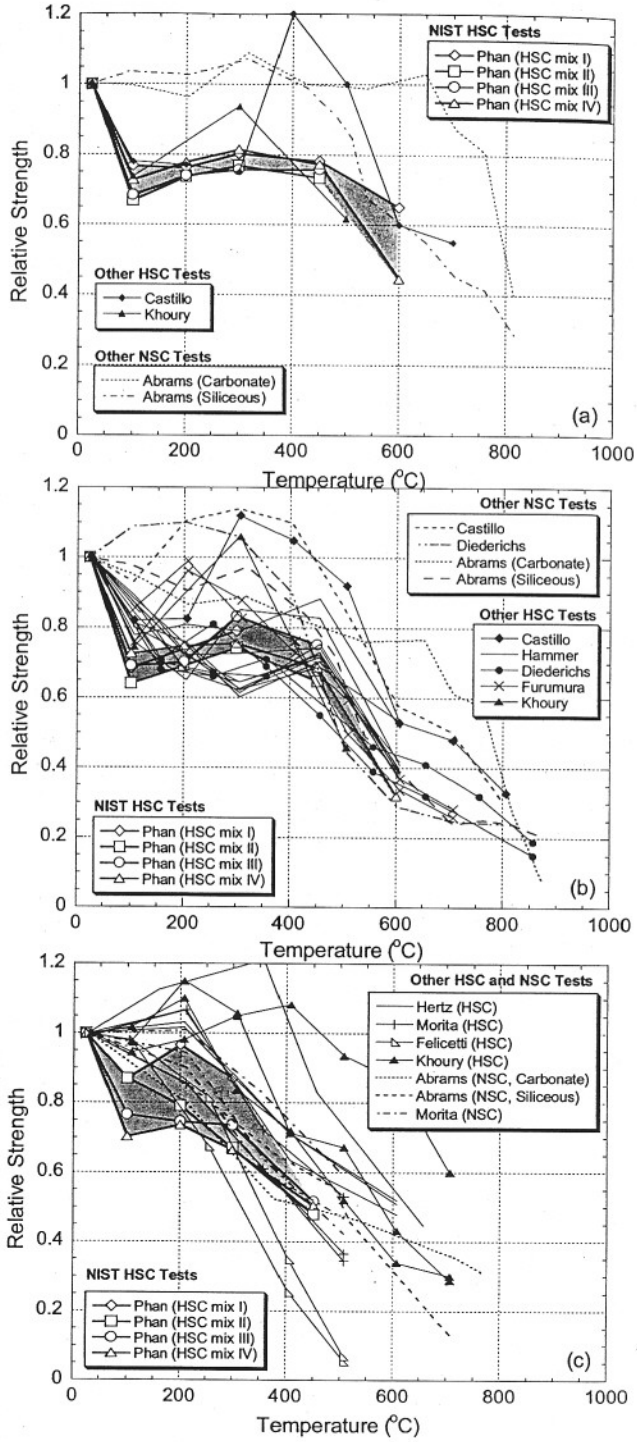

Figure 3. Sstrength-temperature relationships according to (a) Stressed; (b) Unstressed; and (c) Unstressed residual property test method

temperature range of 100 °C to 450 °C. At temperature above 450 °C, both HSC and NSC sustained similar rate of strength loss. More incidences of explosive spalling were observed in the NIST study under the unstressed test method. As a result, NIST mixture I has no strength data above 300 °C, and mixtures II and III have no strength data above 450 °C. Explosive spalling did not occur in any of the mixture IV specimens. Diederichs et al. (1995), Hammer (1995), and Furumura et al. (1995) also reported failure due to explosive spalling of their unstressed HSC specimens, even though some of these studies used very low heating rates (1 °C/min for Furumura and 2 °C/min for Hammer). Study by Castillo and Durrani (1990), however, indicated that explosive spalling occurred only in their stressed test specimens and none occurred under unstressed test method.

Figure 3(c) shows the strength-temperature relationships for the unstressed residual property test. NIST test data showed a wider range of strength loss between the four mixtures under this method than in the stressed or unstressed test methods. The NIST test results at less than 200 °C also differed from data for both HSC and NSC in other studies. The largest difference is at 100 °C, at which the NIST results showed a strength loss ranging between 10 % to 30 %, while data from other studies showed either a strength gain or loss of a little more than 5 %. Above 300 °C, the average difference in relative strengths between test programs appeared to be insignificant. The temperature rates of strength reduction between test programs are also similar. Further, Explosive spalling occurred in one (out of five) NIST mixture I and one (out of four) mixture II specimens while they were being heated to 300 °C. Explosive spalling also occurred in all mixture I specimens while they were being heated to 450 °C. Again, spalling did not occur in any of the NIST mixture IV specimen. Of the referenced studies, only that of Hertz (1984), which used ultra high strength concrete, reported explosive spalling in the unstressed residual property test.

3.1.2 Comparisons with Codes

The above test data are compared with the provisions for concrete strength at elevated temperature by existing codes. Among the codes which specify design rules for computing concrete strength at elevated temperature are the Comité Europeen de Normalisation CEN ENV (1993), the Comites Euro-International du Beton CEB (1991), and the National Building Code of Finnland's RakMK B4 (1991).

CEN ENV and CEB's design provisions make no distinction between HSC and NSC. Thus, their design rules are compared to both HSC and NSC data. Furthermore, while the CEN ENV and the CEB did not explicitly prescribe whether their design rules were specified for concrete in service (i.e. concrete under service load), it is assumed that this is the case since both codes are for the design of structural concrete. Thus, CEN ENV and CEB's design provisions will be compared with the data of the stressed tests.

Finland's *RakMK B4* prescribes different design rules for HSC (with 70 MPa to 100 MPa compressive strength based on 150 mm cubes, or 62 MPa to 90 MPa based on 150 x 300 mm cylinders) and NSC (concretes with 10 MPa to 70 MPa compressive strength based on 150 mm cubes, or 7 MPa to 62 MPa based on 150 x 300 mm cylinders). The RakMK B4 also prescribes different design rules for concrete in service (stressed, $0.3f_{23\ oC}$) and for concrete which is not (unstressed). Thus, the applicability of RakMK B4 will be assessed by comparing with both the *stressed* and *unstressed* test data.

Also, comparisons with *unstressed residual* strength tests will not be made here since the code provisions were prescribed for concrete strength "at" elevated temperature and not for concrete strength at room temperature after exposure to elevated temperature.

Figure 4(a) shows the strength-temperature relationships obtained under the stressed test method in the NIST test program and in studies by Castillo and Durrani (1990), Khoury and Algar (1999) and Abrams (1971). The design rules prescribed by the Eurocodes (for calcareous aggregate and siliceous aggregate concrete) and by the CEB are superposed over the measured strength-temperature relationships for comparison. It should be noted that since carbonate crushed limestones were used as coarse aggregate in the NIST study, the CEN ENV's provision for calcareous aggregate concrete is more applicable for comparison with the NIST results

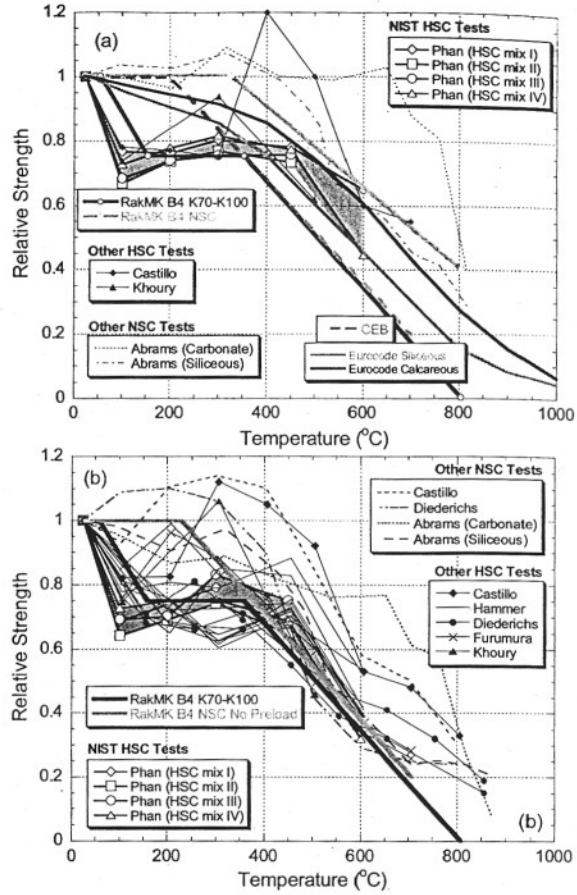

Figure 4. Comparisons of codes with the results of (a) stressed and (b) unstressed tests

As shown in Figure 4(a), the CEN ENV's strength-temperature relationship for calcareous aggregate concrete is un-conservative when used for estimating compressive strength of HSC at temperatures less than 450 °C. The largest overestimation by CEN ENV was by about 20 percent. Above 450 °C, the strength loss prescribed by CEN ENV becomes more consistent with both HSC and NSC data. The unconservative estimation of HSC's compressive strength by CEN ENV at temperatures less than 450 °C is more significant when explosive spalling in the intermediate temperature range is considered. Similarly, CEB's provisions were also based on NSC test data and found to be unconservative when used for estimating HSC compressive strength at temperatures less than 350 °C. The largest overestimation by CEB is by about 25 % at temperatures less than 200 °C. The CEB's rate of strength loss at temperature above 350 °C is consistent with data for both HSC and NSC. As is the case for CEN ENV, the unconservative estimation of HSC compressive strength by CEB at temperatures less than 350 °C is more significant since it does not address the explosive spalling problem in this temperature range. The RakMK B4's provision for in-service concrete (stressed) with K10 to K70 strength grades (NSC) is consistent with the stressed test data for NSC up to 800 °C. The RakMK B4's provision for concrete with K70 to K100 strength grades (HSC) appears to be slightly unconservative at temperatures below 150 °C. However, this is to a much lesser degree compared with the CEN ENV and the CEB. In the intermediate temperature range (150 °C and 350 °C), the RakMK B4's provision for in-service HSC is consistent with the NIST test data. From 350 °C to 800 °C, the RakMK B4

provision appears to be conservative compared with all test data, and is similar to the strength estimation prescribed by CEB.

Figure 4(b) shows the strength-temperature relationships obtained under the unstressed test method and the RakMK B4's strength-temperature relationships for HSC and NSC. Similar to the stressed test, the RakMK B4's strength provision for HSC appears to be slightly unconservative at temperatures below 150 °C with respect to the NIST's test data. However, at temperatures above 150 °C, the RakMK B4's strength predictions are consistent with the NIST test data and the average of all unstressed test results. The RakMK B4's strength prediction for unstressed NSC prescribes a range of no strength loss between room temperature and 220 °C. This is consistent with the average results of tests by Castillo and Durrani (1990), Abrams (1971), and Diederichs et al. (1995). Above 220 °C, RakMK B4 prescribes a strength loss period that has a similar rate of strength reduction as in the case for HSC. The prescribed strength loss is on the conservative side of test results for NSC.

3.2 *Pore Pressure Test Series*

Figures 5 (a) to (e) show the results for a typical pore pressure specimen, in this case specimen I-1.5-13-M-5 (mix I with *w/cm* = 0.22, contained 1.5 kg/m^3 of 13-mm long PP fibers, was moist cured and heated at 5°C/min). The specimen survived the heating exposure without spalling. The results shown in Figure 5 include: (1) pore pressures at points 25 mm and 50 mm from the heated face of the specimen plotted as functions of time (Figure 5 (a)); (2) temperature histories of points inside the furnace (ambient), on the heated face of the specimen, and at 25 mm and 50 mm inside the specimen (Figure 5 (b)); (3) pore pressures at points 25 mm and 50 mm from the heated face of the specimen plotted as functions of temperature (Figure 5 (c)); (4) rate of temperature rise (time derivatives of temperature *dT*/dt, °C/min) plotted as functions of temperature (Figure 5 (d)); and (5) rate of pore pressure rise (time derivatives of pore pressures *dP/dt*, MPa/min) plotted as functions of temperature (Figure 5 (e)). These results, which are discussed in sections that follow, provided insight on the complex heat-induced moisture transport process in concrete and the interdependency between moisture transport and the buildup of pore pressure.

3.2.1 Temperature and Pore Pressure Development

Figures 5 (b) and (d) show the temperature distribution and the time rate of temperature rise, respectively, inside the specimen had a complex history compared with the air temperature. As the air temperature increased, temperatures on the surface and inside the specimen also increased but at varying rates. The changes in the rates of temperature rise (or perturbations) were most pronounced when concrete reached temperatures of about 105°C, 160°C, 180°C, and 220°C. These perturbations are shown as vertical dash lines on Figure 5 (d).

As shown in Figure 5 (d), the time rate of temperature rise (*dT/dt*, °C/min) at point 25 mm from the heated face increased continually to a maximum rate of 1.9 °C/min when the concrete at this location reached 105 °C. At this temperature, free water in the fine concrete pores began to evaporate and diffuse. A portion of the water vapor escaped through the heated surface of the specimen, causing a sudden drop in *dT/dt* on the heated face (see Figure 5 (d)). At the same time, the remaining gaseous mixture of water vapor was transported inward by pressure gradient. This mass transport process (vaporization and diffusion of free water) continued as the temperature inside the concrete increased to about 160 °C. Because of the vaporization and transport of water vapor in this temperature range

(105 °C to 160 °C), the transmission of heat through the concrete is retarded as a result of energy being absorbed in the evaporation process, causing the time rates of temperature rise *dT/dt* at locations inside the concrete to decrease (from 1.9 °C/min to 1.5 °C/min for point at 25 mm deep). During this same temperature range, a noticeable increase in pore pressures, measured at points 25 mm and 50 mm deep, and their corresponding pore pressure rates (*dP/dt*, MPa/min) can be observed as marked by the vertical dashed lines in Figures 5 (c) and (e). As the concrete temperature increased from 160 °C to about 180 °C, a more pronounced drop in *dT/dt* occurred (see Figure 5 (d)). This is believed to be due to the release and diffusion of chemically bound water in the concrete matrix. The additional

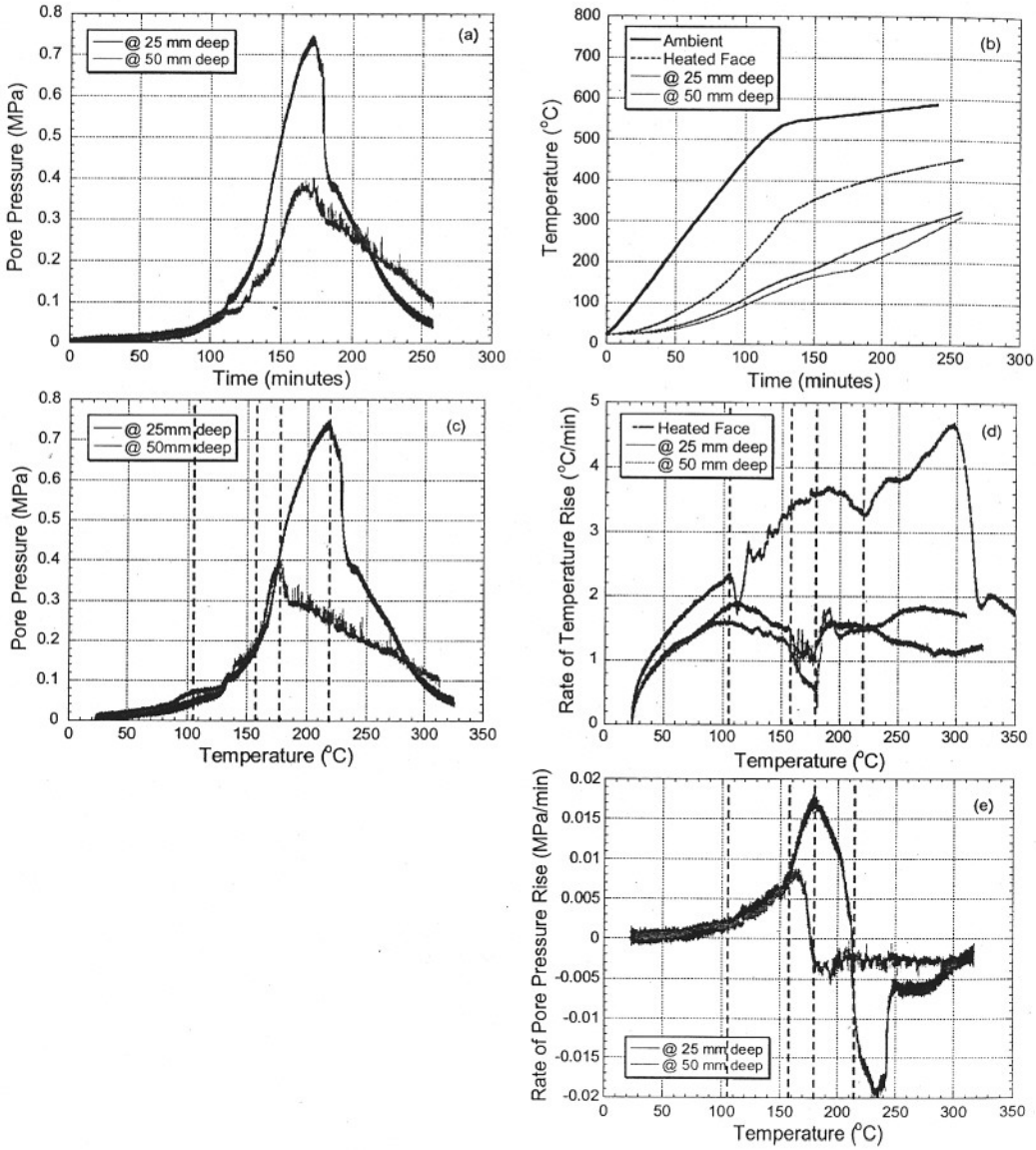

Figures 5 a-e. Test results for I-1.5-13-M-5

volume of water vapor in the concrete pores caused by the release and evaporation of chemically bound water caused a sharp increase in pore pressures and the rates of pore pressure rise *dP/dt* (which reached a maximum of 0.018 MPa/min at 180 °C for point 25 mm deep, see Figure 5 (e)).

Beginning at 180 °C, there was a decrease in *dT/dt* on the heated face of the specimen. This decrease continued until the temperature reached 220 °C, indicating the loss of a significant amount of moisture vapor from the specimen into the furnace in this temperature range (thereby retarding the rate of temperature rise on the concrete surface (see Figure 5 (d)). The escape of moisture vapor caused a sharp drop in *dP/dt* between 180 °C and 220 °C (from 0.018 MPa/min to 0, see Figure 5 (e)). Pore pressure at point 25mm deep continued to increase in this temperature range but at a decreasing rate to a maximum value of 0.75 MPa, while pore pressure at point 50 mm deep had begun to attenuate at the beginning of this temperature range (see Figure 5 (c)). Beyond 220 °C, pore pressure at point 25 mm deep dropped sharply indicating successful attenuation of pore pressure in the specimen (probably due to the presence of PP fibers and microcracks) which prevented explosive spalling from occurring.

The interdependency between temperature and pore pressure described above is consistently observed for all specimens and revealed a complex process of heat-induced moisture transformation and transport that is unique to concrete. The maximum pore pressure measured in the specimens can be found in Phan (2005).

3.2.2 Spalling Characteristics

Specimen I-0-0-M-5 (test #11 in Table 2) and its duplicate (test #12) were the control specimens. They were designed and cured in condition that would result in explosive spalling based on experience with the mechanical property test series. As expected, explosive spalling, which was characterized by the sudden, violent delamination and complete fragmentation of a 20 mm to 30 mm thick concrete layer on the heated surface of the specimen, occurred in both. This was accompanied by an instantaneous release of a large amount of energy that propels the concrete fragments at high velocity, while leaving the remaining portion of the specimen (70 mm to 80 mm thick) intact. This violent and instantaneous delamination and fragmentation is consistent with the notion that explosive spalling failure in HSC results from the build up of internal pore pressure.

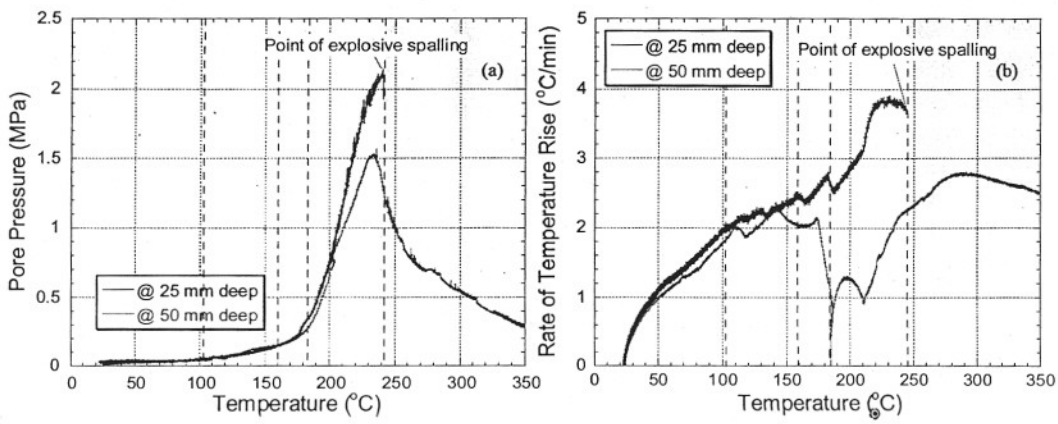

Figure 6. Pore pressure (a) and rate of temperature rise (b) of I-0-0-M-5 vs temperature

Figures 6 (a) and (b) show pore pressures and the time rate of temperature rise dT/dt as functions of temperatures at points 25 mm and 50 mm deep in the control specimen I-0-0-M-5. As can be seen in figure 6 (a), the maximum pore pressure reached just prior to explosive spalling was 2.1 MPa, which was measured at 25 mm deep from the heated face of the specimen. Typically, regardless whether explosive spalling occurred, maximum pore pressure is observed at point about 25 mm deep in all specimens in this test series. Also, as in the case for specimen I-1.5-13-M-5 (see Figures 5 (a) to (e)), perturbations in the time rate of temperature rise at points 25 mm and 50 mm inside this specimen were similarly observed (figure 6 (b)). These perturbations were also marked on Figure 6 (b) by the vertical dashed lines at the temperature levels where it occurred. The corresponding increases in pore pressure were also marked as shown in Figure 6 (a).

3.2.3 Comparisons of Pore Pressure Test Results

Figure 7 shows pore pressure as a function of temperature in the control HSC specimen I-0-0-M-5 and two NSC specimens (IV-0-0-M-5 and IV-0-0-A-5). These specimens are differed by the *w/cm* ratios (between I-0-0-M-5 and IV-0-0-M-5) and curing conditions (between I-0-0-M-5 and IV-0-0-A-5). The influences of *w/cm* and initial moisture content (curing conditions) on pore pressure buildup can be clearly observed. Pore pressure in NSC specimens was able to attenuate gradually after reaching maximum of 1.3 MPa (IV-0-0-M-5) and 0.4 MPa (IV-0-0-A-5), while the control specimen exploded at 2.1 MPa.

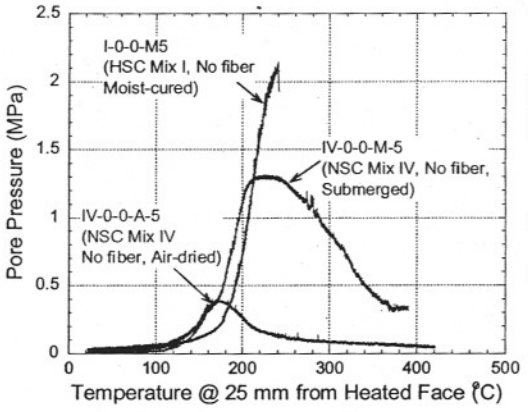

Figure 7. Effects of w/cm and curing conditions

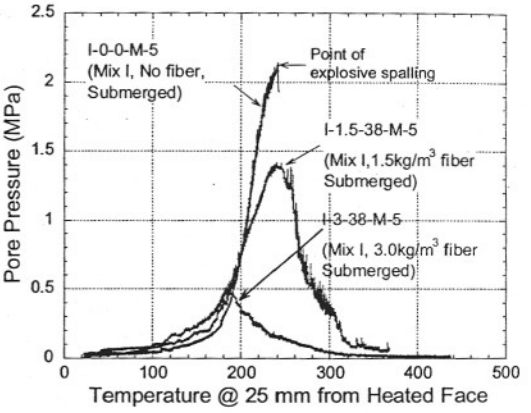

Figure 8. Effects of fiber dosages

Figure 8 shows pore pressures as functions of temperature for three HSC specimens (I-0-0-M-5, I-1.5-38-M-5, and I-3-38-M-5). These specimens are differed only by the amount of PP fibers (no fibers, 1.5 kg/m^3 PP fibers, and 3 kg/m^3 PP fibers, respectively). The effectiveness of PP fibers for pore pressure mitigation can be clearly observed. Instead of reaching the critical pore pressure, the additions of 1.5 kg/m^3 and 3.0 kg/m^3 PP fibers in HSC specimens reduced their maximum pore pressure to levels comparable with those

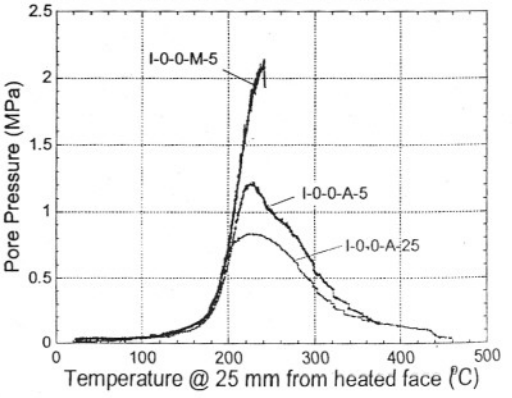

Figure 9. Effects of heating rate

of NSC specimens (shown in Figure 7). Figure 9 shows the effect of heating rate. Consistently, maximum pore pressures in specimens heated at 25 °C/min are lower than those heated at 5 °C/min. In the case shown, specimen I-0-0-A-5 attained a maximum pore pressure of 1.26 MPa while its counterpart (I-0-0-A-25), heated at 25 °C/min, began to attenuate after 0.84 MPa. This is probably due to the higher thermal gradient that caused microcracks to develop and thereby allowing their internal pore pressure to attenuate earlier.

4. Conclusions

The following conclusions can be drawn:

The transformation and mass transport of moisture in concrete have a unique influence on its temperature and pore pressure developments. Noticeable rise in pore pressure occurs when concrete reaches the temperature range of 105 °C to 160 °C (concrete temperature), which coincides with the vaporization of free water and transport of water vapor (as evidenced by the drop in the concrete's rate of temperature rise dT/dt). In the concrete's temperature range of 160 °C and 180 °C, sharp rise in pore pressure occurs. This coincides with the release of chemically-bound water (as evidenced by further drop in dT/dt). Beyond 180 °C, pore pressure continues to rise but with a decreasing rate until peaking in the concrete temperature range from 220 °C to 245 °C. After this point, either explosive spalling occurs or pore pressure attenuates. Spalling pore pressures were measured at 2.1 MPa and 2.02 MPa for the specimens in this study

The additions of PP fibers cause a significant reduction in maximum pore pressure and prevent explosive spalling in specimens that are otherwise identical to the exploded specimens. The highest pore pressure measured for specimens with 1.5 kg/m^3 of PP fibers was 1.42 MPa, a drop of about 45% compared with exploded specimen. For specimens with 3.0 kg/m^3 of PP fibers, this value was 0.66 MPa, a more than 300% drop.

Specimens with high *w/cm* (NSC) and with lower initial moisture contents (cured by air-dried) consistently have lower pore pressure compared with HSC and submerged specimens. Further, thermal gradient is found to be an influencing factor in the process of pore pressure buildup. Higher thermal gradient, caused by high heating rates, might cause microcracks to develop early thereby allowing pore pressure to escape and resulting in lower maximum pore pressure.

HSC that carried a preload equal to 40 % of the room-temperature strength (stressed test) sustained, on average, the smallest strength loss due to temperatures up to 600 °C.

The strength losses measured by the three test methods differed with exposure temperature. For temperatures of 100 °C and 200 °C, *unstressed residual property* test resulted in the lowest strength loss. For exposure to 450 °C, the strength loss was highest for the *residual property* test. These results indicate that there is a complex relationship between the strength measured at elevated temperature and room temperature strength.

Overall, silica fume had no statistically significant effect on the relative strength loss.

The CEN ENV (1993) and CEB (1991)'s strength-temperature relationships are unconservative when applied to HSC.

Finland's RakMK B4 (1991), which considers the differences in concrete strength grades and preload levels, is only slightly unconservative when compared with the test results.

5. References

Abrams, M.S. (1971) Compressive Strength of Concrete at Temperatures to 1600 °F. ACI *SP* ***25***, *Temperature and Concrete*, Detroit, Michigan.

Castillo, C. and Durrani, A. J. (1990) Effect of transient high temperature on high-strength concrete. ACI Materials Journal, v. **87**, no. 1, Jan-Feb, *47-53*.

Comité Européen de Normalisation (1993) prENV 1992-1-2: Eurocode 2: Design of Concrete Structures. Part 1 -2: Structural Fire Design. *CEN/TC 250/SC 2*.

Comites Euro-International Du Beton (1991) Fire Design of Concrete Structures-in accordance with CEB/FIP Model Code 90. *CEB Bulletin D'Information No.* ***208***.

Concrete Association of Finland (1991) High Strength Concrete Supplementary Rules and Fire Design. *RakMK* ***B4***.

Diederichs, U., Jumppanen, U-M., Schneider, U. (1995) High temperature properties and spalling behavior of high strength concrete. *Proceedings, Fourth Weimar Workshop on High Performance Concrete: Material Properties and Design,* Hochschule für Architektur und Bauwesen. Weimar, Germany. *219-236*.

Felicetti, R.; Gambarova, P.G.; Rosati, G.P.; Corsi, F.; Giannuzzi, G. (1996) Residual Mechanical Properties of HSC Subjected to High-Temperature Cycles. *Proceedings, 4th International Symposium on Utilization of HS/HPC* Paris, France, *579-588*.

Furumura, F.; Abe, T.; Shinohara, Y., (1995) Mechanical Properties of HSC at High Temperatures. *Proceedings, 4th Weimar Workshop on HSC: Material Properties and Design*. Hochschule für Architektur und Bauwesen (HAB), Weimar, Germany. *237 - 254*.

Hammer, T.A. (1995) .HIGH-STRENGTH CONCRETE PHASE 3: Compressive Strength and E-modulus at Elevated Temperatures. *SP6* Fire Resistance, Report 6.1, SINTEF Structures and Concrete, STF70 A95023.

Hertz K. (1984) Heat Induced Explosion of Dense Concretes. Institute of Building Design, Report No. 166, Technical University of Denmark.

Kalifa, P.; Menneteau, D.; Quenard, D. (2000) Spalling and Pore Pressure in HPC at High Temperature. *Cement and Concrete Research* 30. *1915-1927*.

Khoury, G.; and Algar, S. (1999) Mechanical behavior of HPC and UHPC concretes at high temperatures in compression and tension. Paper presented at ACI International Conference on State-of-the-Art in High Performance Concrete, Illinois.

Kodur, V.R., (2003) Fiber reinforcement for minimizing spalling in HSC structural members exposed to fire. *Innovations in Fibre-Reinforced Concrete, ACI SP* ***216***. *221-236*.

Malhotra, H.L. (1965) The effect of temperature on the compressive strength of concrete. *Magazine of Concrete Research*, v.**8** (22). pages 85-94.

Morita, T., Saito, H., and Kumagai, H. (1992) Residual mechanical properties of HSC members exposed to high temperature-Part 1: Test on material properties. *Summaries of Annual Meeting*, Architectural Institute of Japan, Niigata.

Phan, L.T. (2005) Pore Pressure in High Strength Concrete at High Temperature. *Proceedings of the Third International Conference on Construction Materials: Performance, Innovations and Structural Implications*. Vancouver, Canada.

Phan, L.T. (2004) Codes and Standards for Fire Safety Design of Concrete Structures in the U.S. *Proceedings of the Workshop on Fire Design of Concrete Structures: What now? What next?*. Milan University of Technology, Milan, Italy. *25-34*.

Phan, L.T.; Carino, N.J. (2003) Code Provisions for High Strength Concrete Strength-Temperature Relationship at Elevated Temperatures. *RILEM Materials and Structures,* v. ***36***. pages 91-98.

Phan, L.T.; Carino, N.J. (2002) Effects of test conditions and mixture proportions on behavior of high-strength concrete exposed to high temperatures. *ACI Materials Journal*, v. **99** (1). pages 54-66.

Schneider U., (1988) Concrete at high temperatures-A general review. *Fire Safety Journal*, The Netherlands. pages 55-68.